

A plasma-membrane E-MAP reveals links of the eisosome with sphingolipid metabolism and endosomal trafficking

Pablo S Aguilar^{1,9}, Florian Fröhlich^{2,9}, Michael Rehman^{2,9}, Mike Shales^{3,9}, Igor Ulitsky^{4,8}, Agustina Olivera-Couto¹, Hannes Braberg³, Ron Shamir⁴, Peter Walter⁵, Matthias Mann⁶, Christer S Ejsing⁷, Nevan J Krogan³ & Tobias C Walther²

The plasma membrane delimits the cell and controls material and information exchange between itself and the environment. How different plasma-membrane processes are coordinated and how the relative abundance of plasma-membrane lipids and proteins is homeostatically maintained are not yet understood. Here, we used a quantitative genetic interaction map, or E-MAP, to functionally interrogate a set of ~400 genes involved in various aspects of plasma-membrane biology, including endocytosis, signaling, lipid metabolism and eisosome function. From this E-MAP, we derived a set of 57,799 individual interactions between genes functioning in these various processes. Using triplet genetic motif analysis, we identified a new component of the eisosome, *Eis1*, and linked the poorly characterized gene *EMP70* to endocytic and eisosome function. Finally, we implicated *Rom2*, a GDP/GTP exchange factor for *Rho1* and *Rho2*, in the regulation of sphingolipid metabolism.

The plasma membrane is the defining feature of the cell, separating its interior from the exterior space. It controls exchange and communication processes between the cell and its environment. The delivery of cellular material to the plasma membrane or cell exterior is mediated by exocytosis. Conversely, endocytosis is used to take up plasma membrane and external components. In addition, many signaling processes occur at the plasma membrane simultaneously and are often regulated by the endocytosis of receptors or delivery of messenger molecules. To coordinate these processes and maintain cell integrity under changing conditions, both plasma-membrane protein and lipid composition are regulated and adjusted to external conditions. Despite impressive advances in our understanding of these individual processes, it is not well understood how they are coordinated.

To accommodate its many functions, the plasma membrane is highly organized, both spatially and temporally. In *Saccharomyces cerevisiae*, several plasma-membrane domains of different composition are distinguishable by light microscopy. This organization is mediated, at least in part, by eisosomes, large protein complexes that underlie one of the domains, named MCC after the marker protein *Can1* found there. When *PIL1*, encoding a major eisosome component, is deleted, cells have abnormal plasma-membrane structure with large invaginations and loss of MCC protein organization^{1,2}. In addition, the endocytosis of several plasma-membrane proteins is either accelerated or delayed^{2,3}. The molecular function of eisosomes is still unknown, but recent data show that they interact with

sphingolipid-regulated Pkh-kinases, which phosphorylate their core components and are required for efficient endocytosis⁴⁻⁶. In addition to Pkh-kinases, Tor kinase complex 2 (TORC2) is implicated in sphingolipid metabolism regulation⁷. However, it is unclear how these different signaling pathways are controlled and coordinated as well as what their downstream effects are. Experimental evidence supports a model in which regulation of sphingolipid, sterol and glycerophospholipid levels in the plasma membrane are coordinated, but mechanistic insights as to how this is achieved are currently lacking^{8,9}. To reveal functional links between the different processes, we generated a quantitative genetic-interaction map targeting a large set of genes implicated in plasma-membrane function.

Genetic interactions have long been used to dissect functional relationships between genes. Classically, researchers have looked for qualitative differences between observed phenotypes of double mutants and the phenotypes of the two related single mutants. More recently, we employed the epistatic miniarray profile (E-MAP) approach, a variation on synthetic genetic arrays¹⁰. This allows for the quantitative analysis of genetic interactions, including negative (for example, synthetic sick or lethal) as well as positive ones (for example, suppression)¹¹. For this approach, a comprehensive set of double mutants is generated and their growth is measured. To determine individual genetic interactions, deviations of growth rates from the medians of all combinations with one particular gene are calculated for each combination as a quantitative interaction score

¹Institut Pasteur de Montevideo, Montevideo, Uruguay. ²Max Planck Institute of Biochemistry, Organelle Architecture and Dynamics, Martinsried, Germany. ³Department of Cellular and Molecular Pharmacology, University of California, San Francisco, California, USA. ⁴The Blavatnik School of Computer Science, Tel Aviv University, Tel Aviv, Israel. ⁵Department of Biochemistry and Biophysics, University of California and Howard Hughes Medical Institute, San Francisco, California, USA. ⁶Max Planck Institute of Biochemistry, Proteomics and Signal Transduction, Martinsried, Germany. ⁷University of Southern Denmark, Department of Biochemistry and Molecular Biology, Odense, Denmark. ⁸Present address: Whitehead Institute for Biomedical Research, Cambridge, Massachusetts, USA. ⁹These authors contributed equally to this work. Correspondence should be addressed to N.J.K. (krogan@cmp.ucsf.edu) or T.C.W. (twalther@biochem.mpg.de).

Received 10 December 2009; accepted 9 April 2010; published online 6 June 2010; doi:10.1038/nsmb.1829

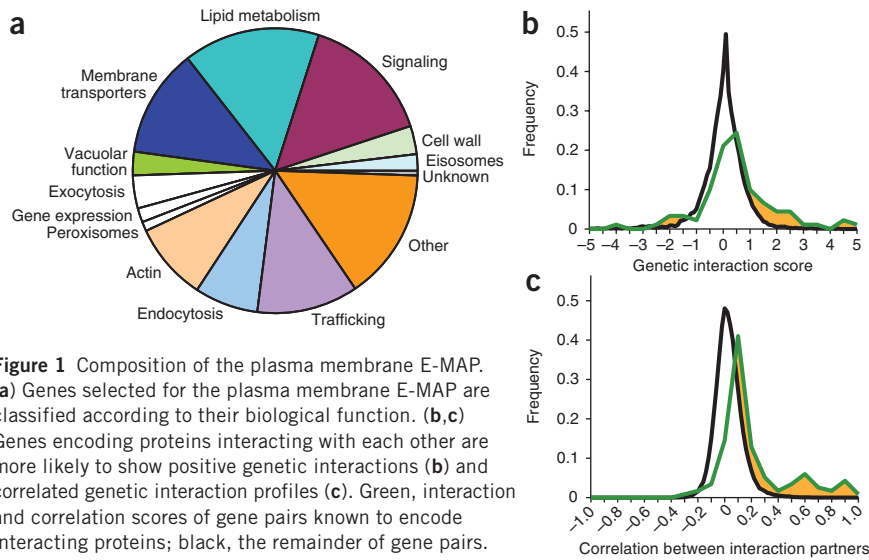


Figure 1 Composition of the plasma membrane E-MAP. (a) Genes selected for the plasma membrane E-MAP are classified according to their biological function. (b,c) Genes encoding proteins interacting with each other are more likely to show positive genetic interactions (b) and correlated genetic interaction profiles (c). Green, interaction and correlation scores of gene pairs known to encode interacting proteins; black, the remainder of gene pairs.

(or S-score)^{12,13}. Each mutation has a genetic-interaction profile, or phenotypic signature, consisting of all its S-scores with all other genes in the E-MAP. A particularly useful parameter to judge the similarities of profiles is to compare correlations of two genes' interactions with all other genes in the set. In addition, bioinformatic extraction based on mathematical models can be applied to yield functional modules in an unbiased fashion from E-MAP datasets, and correlations and S-scores can be used to reveal their connections^{14,15}. The E-MAP approach has been previously used to functionally interrogate several processes, and the dissection of genetic interactions from these E-MAPs has led to a deluge of biological insights in a variety of processes^{11,16–18}.

Here we report an E-MAP targeting plasma-membrane functions to generate previously unknown biological insight relating to plasma-membrane functions. Using this E-MAP, we have linked two new genes (*EMP70* and *EIS1*) to eisosome function and uncovered a link between GDP/GTP exchange protein Rom2 signaling and sphingolipid metabolism.

RESULTS

Overview of the plasma-membrane E-MAP

To address functional relationships between plasma-membrane processes, we systematically determined the genetic interactions among a set of 374 genes involved in plasma-membrane biology. We selected candidate genes encoding proteins functioning in membrane transport and organization, especially eisosomes, actin patches, endocytosis and exocytosis. In addition, we picked genes involved in ergosterol and sphingolipid metabolism, as these lipids are implicated in many plasma-membrane processes. Our selection criteria were based on available functional annotation (gene ontology terms) and a literature survey. We also included a diverse set of genes whose products localize to the plasma membrane and/or interact genetically or physically with previously characterized plasma-membrane genes/proteins. The selected genes were categorized into the functional groups presented in **Figure 1a** and **Supplementary Table 1**. We included a number of genes analyzed in previous systematic genetic studies to facilitate comparison between datasets^{11,16,17}. From this set, we quantitated a total of 57,799 genetic interactions using the E-MAP approach (~83% of the possible interactions).

Previously, we found that gene pairs encoding physically interacting proteins are enriched for positive genetic interactions and show a higher propensity for having highly correlated genetic-interaction profiles^{11,16,17}. To assess the richness and quality of the genetic-interaction data of the plasma-membrane E-MAP, we compared the

pairwise correlation of genetic-interaction profiles to a high-quality set of protein-protein interactions (PPIs)¹⁹ and found that the power of the genetic map to predict PPIs is comparable to that of previously published E-MAPs (**Supplementary Fig. 1**). Furthermore, comparison of interaction scores or correlation coefficients of gene pairs encoding physically interacting proteins^{19–21} (see **Supplementary Table 2**) among all plasma-membrane E-MAP gene pairs revealed that they have a higher likelihood to interact positively and to have correlated genetic-interaction profiles (**Fig. 1b,c**, yellow area under the green graph). Conversely, gene pairs with highly correlated interaction profiles and positive interactions are likely to physically interact.

To better visualize groups of interacting genes and their relationships, we used a previously developed algorithm that defines functional modules from quantitative genetic and PPI data¹⁴ (**Supplementary Fig. 2**). This method identified 18 modules encompassing 53 genes (**Supplementary Fig. 2** and **Supplementary Table 3**). Genes in each module have similar genetic-interaction profiles and form a connected subnetwork in the PPI network. These modules corresponded to known protein complexes, such as the F-actin capping protein complex and the AP-3 adaptor, or to known pathways, such as sphingolipid metabolism, the HOG osmosensory pathway and ergosterol biosynthesis (**Supplementary Fig. 2**). To identify modules for which PPI data is not available, we performed the modular analysis without requiring PPI connectivity (**Supplementary Fig. 3**). This identified 29 modules encompassing 190 genes (**Supplementary Table 4** and <http://acgt.cs.tau.ac.il/pmemap>). This analysis yielded similar amounts of modules for the plasma membrane and the previously reported E-MAP on the early secretory pathway¹¹ (**Supplementary Table 5**). Additional information can be extracted by considering interactions of single genes with modules (data not shown).

Insights from hierarchical clustering of the genetic-interaction data

Each mutant engenders a genetic-interaction profile, or phenotypic signature, representing how it genetically interacts with all other mutants tested. Comparison of these profiles using hierarchical clustering (**Fig. 2**, **Supplementary Data** and http://interactome-cmp.ucsf.edu/plasma_membrane/) is a powerful and unbiased approach to identify genes of the same pathway. In the following, we provide a brief summary of several functional connections revealed by such gene clustering.

RVS161 and *RVS167* encode proteins that operate together in membrane remodeling during endocytosis²². As expected from their overlapping functions, *rvs161Δ* and *rvs167Δ* clustered together with high correlation (correlation = 0.54; **Fig. 2**, inserts 2). Consistent with previous reports, both share positive genetic interactions with a number of genes involved in fatty-acid elongation for sphingolipid synthesis, such as *FEN1* and *SUR4* (ref. 23) (**Fig. 2**, insert 2d). Notably, we observed positive interactions with genes encoding components of the Hog1 MAP-kinase cascade and the ergosterol biosynthesis pathway (*erg3Δ*, *erg5Δ*, *erg6Δ*, **Fig. 2**, inserts 2). In additions to changes in their sterols, these *erg* mutants have altered sphingolipid composition⁸. Thus, defects resulting from deletion of *RVS* genes could be compensated by *erg* mutants via changes in sphingolipids. Also in line with previous work, both *rvs161Δ* and *rvs167Δ* show negative interactions with actin

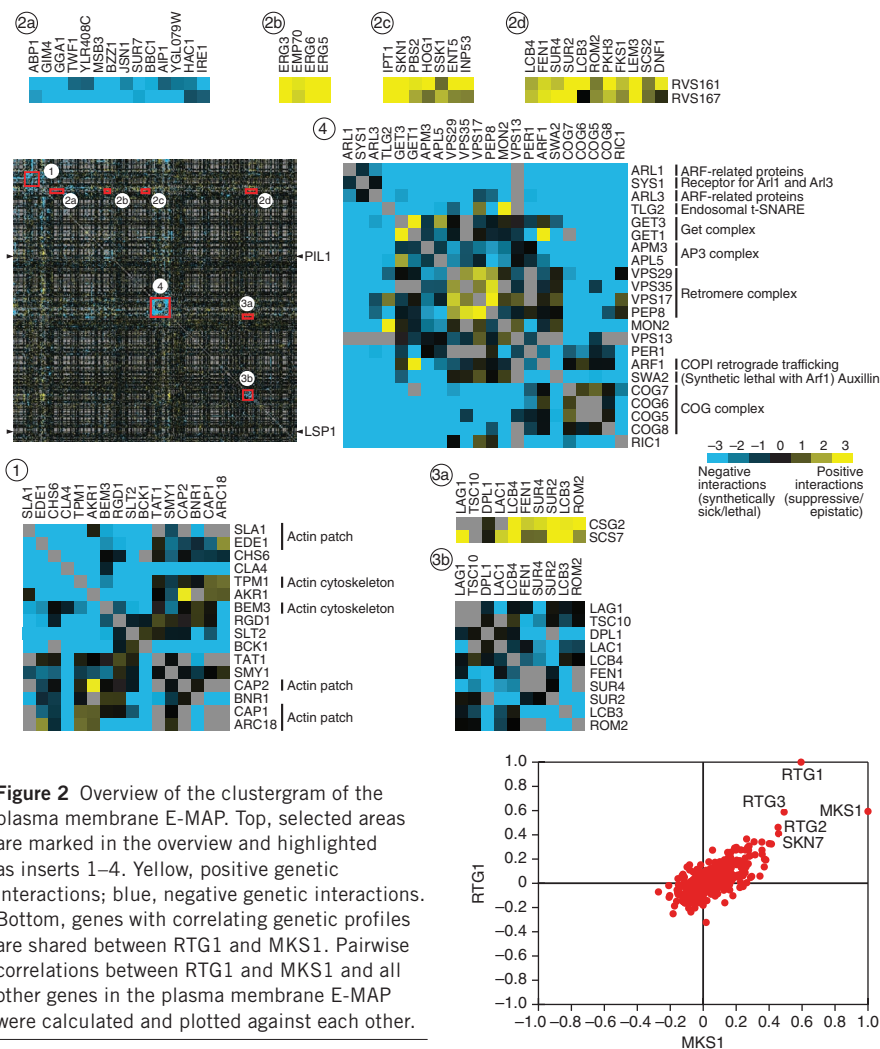


Figure 2 Overview of the clustergram of the plasma membrane E-MAP. Top, selected areas are marked in the overview and highlighted as inserts 1–4. Yellow, positive genetic interactions; blue, negative genetic interactions. Bottom, genes with correlating genetic profiles are shared between RTG1 and MKS1. Pairwise correlations between RTG1 and MKS1 and all other genes in the plasma membrane E-MAP were calculated and plotted against each other.

cytoskeleton genes, such as *BBC1*, *JSN1* and *BZZ1* (refs. 10,24–26) (Fig. 2, insert 2a). In addition, we found several previously unrecognized relationships, including negative interactions between the *RVS* genes and *ire1Δ* and *hac1Δ*, two mediators of the unfolded protein response (UPR) control system for endoplasmic reticulum function. Possibly, cells react to Rvs deficiency by altering lipid synthesis or transport, which in turn activates the UPR. Cells lacking the UPR in addition to the Rvs proteins could have decreased fitness. Consistent with this notion, a recent genome-wide study found the UPR activated in *rvsΔ* cells²⁷.

We also detected many genetic interactions and highly correlated profiles between genes encoding actin-patch components. For example, *sla1Δ* and *ede1Δ*, which function in endocytosis, are highly correlated (correlation = 0.64, Fig. 2, insert 1) and show a negative genetic interaction (interaction score = -7.7). Unexpectedly, given its function in exocytosis rather than endocytosis, we also found *chs6Δ* to be highly correlated with *sla1Δ* and *ede1Δ* (correlations *ede1Δ-chs6Δ* = 0.53 and *sla1Δ-chs6Δ* = 0.43; Fig. 2, insert 1). Furthermore, these three genes all result in negative genetic interactions when any two of them are combined. Collectively, this indicates that Chs6 might function in coordinating exo- and endocytosis, perhaps by delivering a subset of cargos to the plasma membrane²⁸. In this scenario, *chs6Δ* would lead to the depletion of an endocytic factor from the plasma membrane and, as a consequence, a decrease in endocytosis efficiency. Combination with mutants defective in

this process would further decrease the fitness of the resulting strains.

We also observed many strong genetic interactions between trafficking complexes. Genes encoding the retromer complex (*VPS17*, *VPS29*, *VPS35*, *PEP8*), the COG complex (*COG5*, *COG6*, *COG7*, *COG8*) or the AP3 complex (*APM3*, *APL5*) all formed highly correlated clusters in the plasma-membrane E-MAP (Fig. 2, insert 4). In addition, potential new connections between these complexes and heretofore poorly characterized components of the endocytic machinery are apparent in these clusters. As an example, the retromer complex coclusters with deletion of *MON2* (correlation = 0.48), a gene encoding an evolutionarily conserved scaffolding protein functioning in endosome-to-Golgi trafficking²⁹. Our data suggest that Mon2 acts together with the retromer in this process.

Many genes encoding members of signaling cascades showed strong genetic relationships. For example, two kinases of the cell integrity MAP kinase signaling module, *Slt2* (the MAP kinase) and *Bck1* (the MAP kinase kinase)³⁰, showed one of the highest correlations (0.75). Similarly, genes encoding components of retrograde signaling (*RTG1*, *RTG2*, *RTG3* and *MKS1*) all cluster together (correlation = 0.44) indicating that all pairs have high correlation coefficients (for example, *MKS1/RTG1* correlation coefficient = 0.59; Fig. 2, bottom).

Functional links involving eisosomes

Although the eisosome has been linked to endocytosis regulation, details regarding its biological roles remain unresolved. To understand eisosome function *in vivo*, we genetically analyzed its core components, *PIL1* and *LSP1*. As the encoded proteins are >70% identical and are stoichiometric components of the eisosome, we expected very similar genetic profiles for them. Unexpectedly, *PIL1* and *LSP1* showed very different genetic interactions and, accordingly, cluster in different regions of the E-MAP (correlation = 0.038; Fig. 2, insert 4). This parallels the cell-biological observation that deletion of *PIL1* but not *LSP1* results in strong effects on plasma-membrane organization and protein turnover.

To gain further insight into eisosome function, we analyzed the triplet genetic motifs (TGMs) in which *pil1Δ* participates¹⁷. TGMs are the simplest motifs apart from binary interactions and can exist in four forms: type I (all three genes showing positive genetic interactions), type II (two positive and one negative), type III (two negative and one positive) and type IV (three negative interactions) (Fig. 3a). We have previously shown that genes with all positive genetic interactions (type I TGM) are enriched for functioning in the same pathway¹⁷. We therefore assembled a complete map of type I TGMs found in the plasma-membrane E-MAP (Supplementary Fig. 4). Because Pil1 has a more prominent role than Lsp1 in eisosome and plasma-membrane function, we extracted all type I TGMs involving *pil1Δ* (Fig. 3b). In this representation, we highlighted genes that are important for eisosome localization or are closely related to such genes (*YMR031c* and *EMP70*, respectively³¹; green nodes in Fig. 3b) and characterized them further.



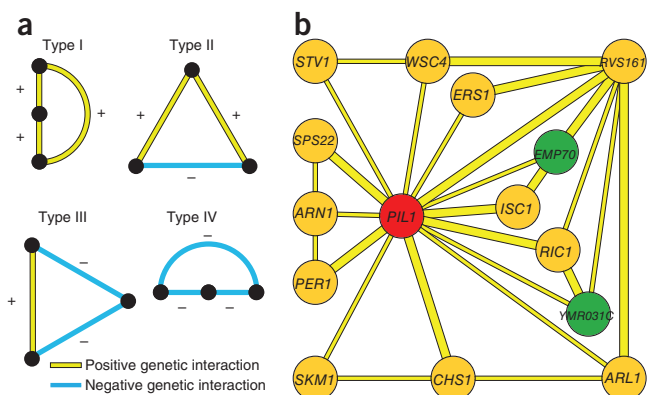


Figure 3 TGMs of the plasma membrane E-MAP. **(a)** All four potential TGMs are shown. Nodes in vertical order represent involvement in the same pathway; horizontal orientation indicates possible parallel pathways. **(b)** Type I TGMs that have *PIL1* as a node. Nodes in green represent a gene important for Pil1-GFP localization (*YMR031C*) or a homolog of such a gene (*EMP70*)³¹.

***EIS1/YMR031c* encodes a novel eisosome component**

Because *ymr031cΔ* and *pil1Δ* have a positive genetic interaction and a correlated interaction profile (Fig. 3b), we tested whether the corresponding proteins physically associate. To this end, we fused the sequence encoding the green fluorescent protein (GFP) tag to *PIL1* at its endogenous location in the yeast genome and immune-purified the expressed Pil1-GFP from a yeast culture that was metabolically labeled with heavy, nonradioactive lysine (SILAC)³². In parallel, we performed a mock purification from control, light-labeled wild-type cells. We identified 533 proteins present over a 10,000-fold dynamic range in the mixed eluates from both purifications. As expected, we found Pil1 and Lsp1 as well as the recently identified eisosomes binding protein Mrp8 to be significant outliers, with a high ratio of labeled

to nonlabeled protein, indicating that they are specific interactors^{2,33} ($P < 0.0001$; Fig. 4a). In addition, we found a number of other specific interactors, including Ymr031c, which is consistent with a recent report³⁴. To independently confirm this observation, we performed immunoprecipitations of TAP-tagged Ymr031c and, as a control, Lsp1, and we found that both specifically precipitated Pil1 (Fig. 4b). To test whether Ymr031c colocalizes with Pil1, we fluorescently tagged both proteins. The signal from Pil1 and Ymr031c perfectly overlapped at eisosomes (Fig. 4c, upper panel; Pearson correlation = 0.81 ± 0.06). Consistent with these data, Ymr031c was recently detected at MCCs³. One prediction for a genuine eisosome component is that it relocates to eisosome remnants in a *PIL1* deletion strain². We therefore investigated Ymr031c-GFP localization in *pil1Δ* cells and found that both Ymr031c and the eisosome component Lsp1 localized to one or a few eisosome remnants in the cell periphery (Fig. 4d). To investigate whether *YMR031c* has a role in eisosome architecture or assembly, we deleted it and analyzed the localization of eisosome core components in the resulting strain. For both Pil1 and Lsp1-GFP, we observed substantially increased cytosolic fluorescence in *ymr031cΔ* cells (Fig. 4e,f). Collectively, these data show that Ymr031c is physically associated with eisosomes and is required for their normal formation. We have therefore named this gene *EIS1*.

***EMP70* is an early endosomal and vacuolar protein**

In the genetic network of the plasma-membrane E-MAP, *EMP70* is the strongest candidate for a functional relationship with *PIL1* because (i) the two genes have highly correlated genetic profiles (correlation of *PIL1* and *EMP70* = 0.37 (*EMP70* has the most similar profile to *PIL1* of all the E-MAP genes); Fig. 5a); (ii) the two genes participate in two type I TGMs (Fig. 3b); and (iii) the *Emp70* homolog Tmn2 is required for normal Pil1-GFP localization³¹. In addition, our modular analysis identified *EMP70* and *PIL1* as part of the same six-gene module (Supplementary Fig. 3; S-score between *PIL1* and *EMP70* = 1.78; Supplementary Table 4).

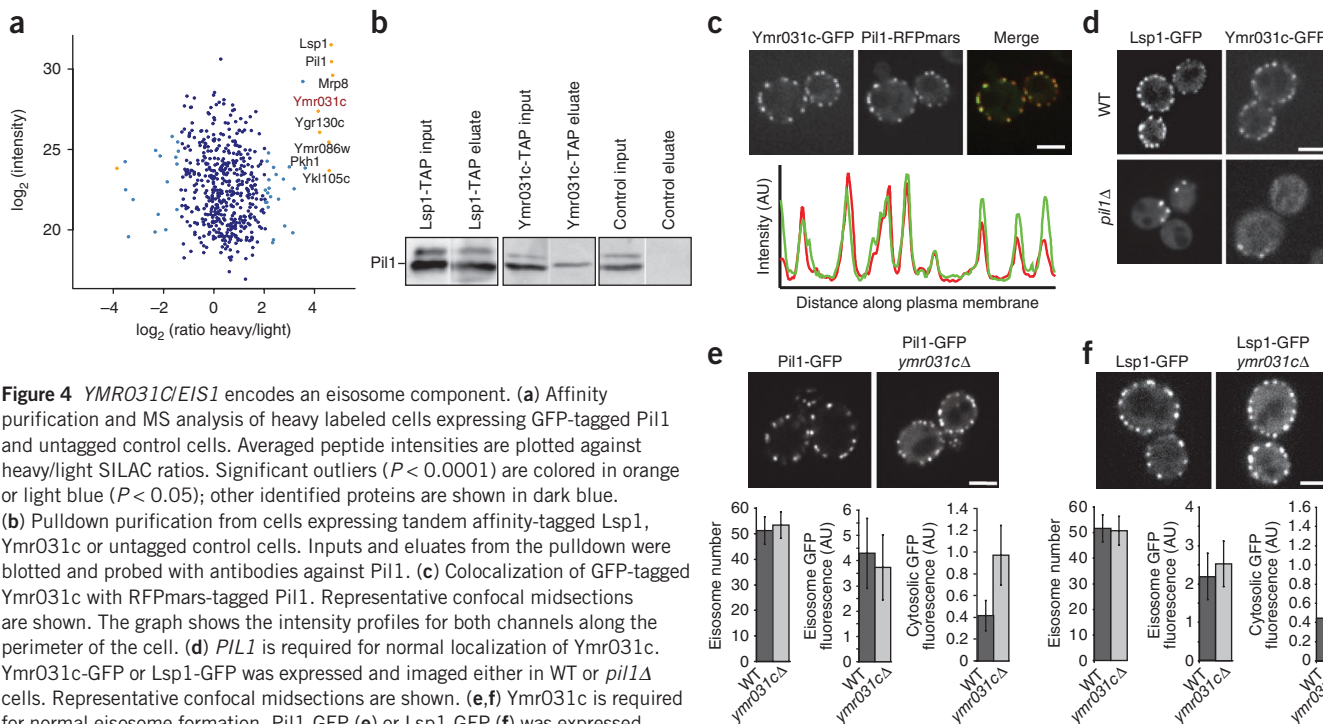
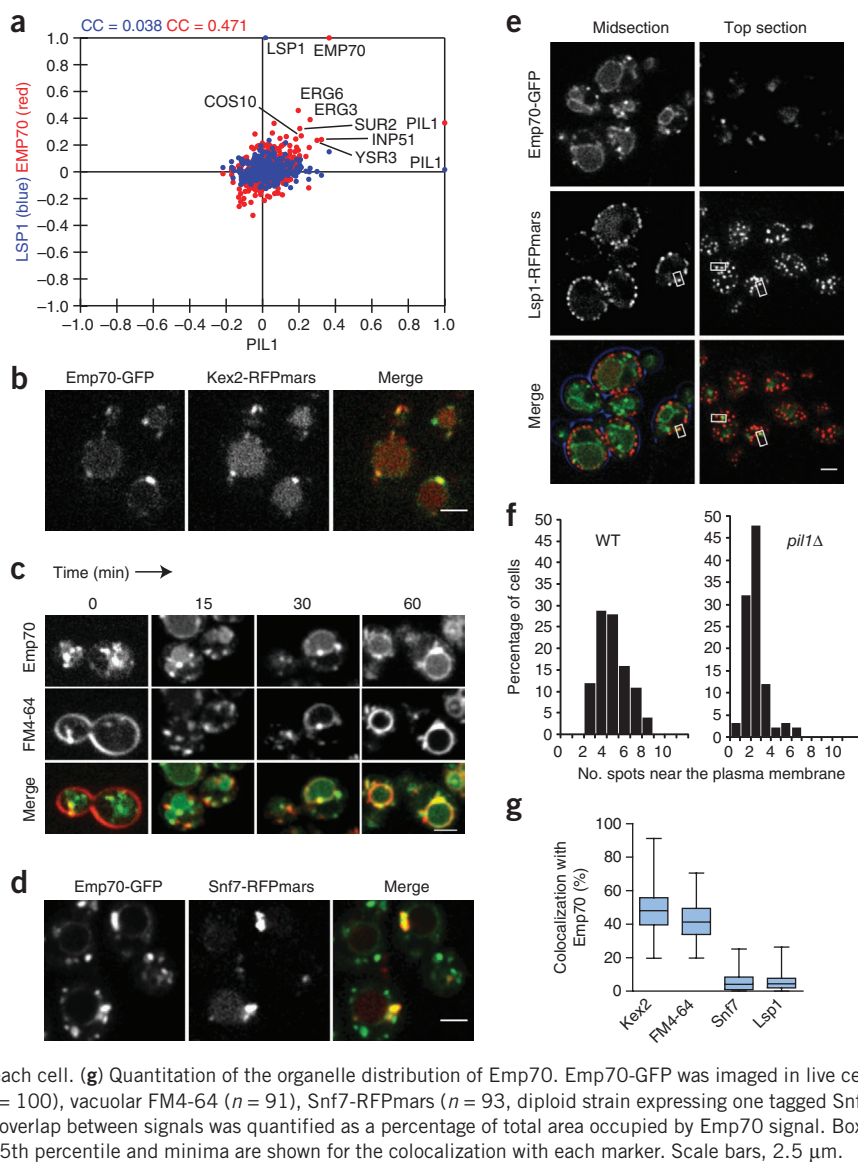


Figure 4 *YMR031C/EIS1* encodes an eisosome component. **(a)** Affinity purification and MS analysis of heavy labeled cells expressing GFP-tagged Pil1 and untagged control cells. Averaged peptide intensities are plotted against heavy/light SILAC ratios. Significant outliers ($P < 0.0001$) are colored in orange or light blue ($P < 0.05$); other identified proteins are shown in dark blue. **(b)** Pull-down purification from cells expressing tandem affinity-tagged Lsp1, Ymr031c or untagged control cells. Inputs and eluates from the pull-down were blotted and probed with antibodies against Pil1. **(c)** Colocalization of GFP-tagged Ymr031c with RFPmars-tagged Pil1. Representative confocal midsections are shown. The graph shows the intensity profiles for both channels along the perimeter of the cell. **(d)** *PIL1* is required for normal localization of Ymr031c. Ymr031c-GFP or Lsp1-GFP was expressed and imaged either in WT or *pil1Δ* cells. Representative confocal midsections are shown. **(e,f)** Ymr031c is required for normal eisosome formation. Pil1-GFP **(e)** or Lsp1-GFP **(f)** was expressed in *ymr031cΔ* or control cells. Representative midsections are shown. For each experiment, the number of eisosomes per cell, the GFP fluorescence per eisosome and the cytosolic GFP fluorescence were quantified from at least 100 cells and are shown below the images. Scale bars, 2.5 μm.

Figure 5 The eisosome-linked Emp70 is an early endosomal protein. **(a)** Genes with correlating genetic profiles are shared between *PIL1* and *EMP70* but not *PIL1* and *LSP1*. Correlation coefficients between the genetic profile of *PIL1* and each of the other 373 profiles in the E-MAP are plotted on the x axis against, on the y axis, either the similar set of values for the *LSP1* profile with all other profiles (blue) or those for *EMP70* with all other profiles (red). Labeled points indicate some genes with profiles that are positively correlated with both the profile of *PIL1* and that of *EMP70*. CC values in blue and red indicate the correlation coefficients for the full set of blue or red points plotted. **(b)** Emp70 colocalizes with Kex2. Emp70-GFP and Kex2-RFPmars were coexpressed and imaged. Representative confocal midsections are shown. **(c)** Emp70 localizes to an FM4-64 marked endocytic compartment. Cells expressing Emp70-GFP (green) were pulse labeled with FM4-64 (red) and imaged for 1 h. Images of midsections of cells at selected time are shown as indicated. **(d)** Emp70 localizes to the class E compartment in *SNF7* mutants. GFP-tagged Emp70 was expressed in cells harboring nonfunctional Snf7-RFPmars, resulting in the clustering of endosomal proteins in the class E compartment. Representative confocal midsections are shown. **(e)** Emp70-GFP foci localize to the cell periphery. Emp70-GFP (green) was expressed in cells harboring the fluorescent eisosomes marker Lsp1-MARS. Representative mid- (left) and top sections (right) are shown. Boxes highlight selected areas of colocalization. **(f)** *PIL1* is required for normal Emp70 localization to the cell periphery. Emp70-GFP was expressed in cells expressing the plasma membrane marker Ylr413w-RFPmars, and foci overlaying this marker were counted in more than 100 WT and *pil1Δ* cells. Results are shown as a histogram of number of spots opposed to the plasma membrane in each cell. **(g)** Quantitation of the organelle distribution of Emp70. Emp70-GFP was imaged in live cells and analyzed for colocalization with Kex2-RFPmars ($n = 100$), vacuolar FM4-64 ($n = 91$), Snf7-RFPmars ($n = 93$, diploid strain expressing one tagged Snf7 allele) and Lsp1-Cherry ($n = 107$). The relative area of overlap between signals was quantified as a percentage of total area occupied by Emp70 signal. Box plots representing maxima, 75th percentile, median, 25th percentile and minima are shown for the colocalization with each marker. Scale bars, 2.5 μm .



These genetic links prompted us to investigate *EMP70* in more detail (Fig. 5). We fluorescently tagged Emp70 with GFP and found that it localizes in a complex pattern consisting of a central ring reminiscent of vacuoles and several bright foci in the cytoplasm that often seem connected to the vacuole (Fig. 5b and Supplementary Video 1). Emp70 was previously found in an endosomal membrane fraction³⁵. We therefore tested whether cytosolic Emp70 foci represent endosomes. We used a number of endosomal markers and found Emp70-GFP foci to colocalize with Kex2, marking the early endosome, which in yeast is functionally continuous with the trans-Golgi network. In contrast, Emp70 localization did not overlap with the late endosomal/prevacuolar marker Vps5 (Fig. 5b and Supplementary Fig. 5a).

To test whether the Emp70-labeled compartments are part of the endocytic route, we used the endocytosis tracer FM4-64. This lipid dye is incorporated in the plasma membrane, taken up by endocytosis and trafficked through the endosomal system to the vacuole³⁶. We found in pulse-chase experiments that early FM4-64 intermediates colocalize with Emp70 foci (Fig. 5c, 0 min). As the dye migrated through the endocytic system, it also colocalized with a subset of Emp70-positive foci toward the end of the reaction but markedly less

at intermediate time points (Fig. 5c, 30 min). At the final time point, FM4-64 clearly labeled the vacuole delimiting membrane where it colocalized with the Emp70-GFP ring staining. Trafficking from early endosomes can be blocked by incubation of cells at 16 °C, which leads to the accumulation of FM4-64 (ref. 37). Emp70-GFP almost perfectly colocalized with FM4-64 when the latter was accumulated in such a '16 °C compartment', further arguing that Emp70 localizes to early endosomes (Supplementary Fig. 5b). Strains harboring a deleted or C-terminally tagged *SNF7* (an ESCRT-III gene) show a 'class E' vacuolar protein sorting defect. This is characterized by collapse of endosomes to one or a few large class E compartments^{38,39}. Under these conditions, Emp70-GFP formed fewer, very large clusters that colocalized with Snf7-RFPmars marked class E compartments and showed reduced vacuolar membrane staining (Fig. 5d). From these data, we conclude that Emp70 localizes to early endosomes and the vacuole. To better characterize the localization of Emp70 in these two pools, we quantitated the relative amount of Emp70 colocalizing with markers for each organelle and found 48% of Emp70 to localize in the TGN/endosomal compartment and 41% at the vacuolar membrane (Fig. 5g).



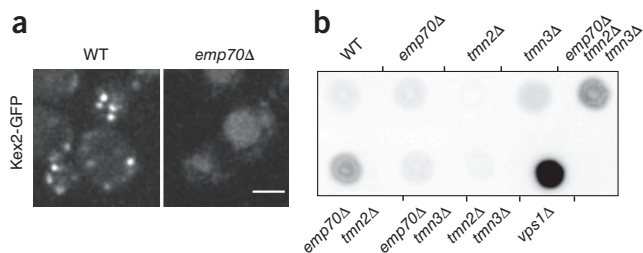


Figure 6 Emp70 is required for normal endosome function. (a) *EMP70* is required for normal localization of Kex2-GFP. Kex2-GFP was expressed in either WT or *emp70Δ* cells, and representative confocal midsections are shown. (b) Emp70 family members are required for late endosomal protein retrieval. Mutants of *EMP70*, *TMN2* or *TMN3* were tested alone or in combination for CPY secretion. A representative colony blot is shown. Scale bar, 2.5 μm.

During our localization studies, we often observed early endosomal foci marked by FM4-64 dynamically associating with the plasma membrane. To test whether the genetic link of *EMP70* with *PIL1* was reflected in the recruitment of Emp70-GFP foci to eisosomes, we investigated the Emp70-GFP localization with respect to fluorescently tagged eisosomes. Strikingly, we found many spots of Emp70-GFP at eisosomes (Fig. 5e). In any given cell, 4% of the total Emp70-GFP signal colocalized with an eisosome marker (Fig. 5g and Supplementary Video 2). To test whether this association has functional relevance, we investigated the Emp70 localization in *pil1Δ* cells and found a marked reduction of foci close to the plasma membrane (Fig. 5f).

EMP70 proteins are required for normal endosomal sorting

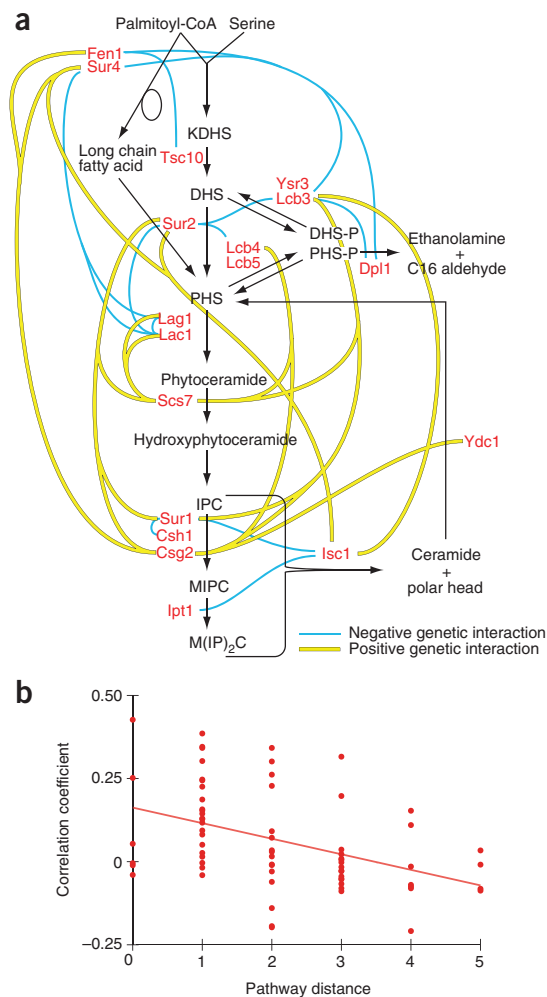
To test whether Emp70 is important for early endosome-to-vacuole trafficking, we analyzed Kex2-GFP localization in an *emp70Δ* strain and found a substantial Kex2 relocalization from early endosomes to the vacuole (Fig. 6a). Kex2 steady-state localization depends on signals that send it to early endosomes, which subsequently mature into late endosomes, from which Kex2 is actively retrieved^{40,41}. It is possible that vacuolar mislocalization of Kex2 in *emp70Δ* cells results from a defect in retrieval from the late endosome or a complex-trafficking problem affecting early endosome function. Normally, if retrieval is compromised, vacuolar sorted carboxypeptidase Y (CPY) is secreted. We tested this and found that, in contrast to the control *vps1Δ*, *emp70Δ* alone does not lead to CPY secretion^{42,43}. *EMP70* has two homologs in the genome, *TMN2* and *TMN3*. To address whether they could compensate for Emp70 function in its absence, we tested CPY secretion in strains with different combinations of the family members deleted. *TMN2* deletion alone had no effect, and *TMN3* deletion alone only a weak effect, on CPY sorting (Fig. 6b). In contrast, combining *emp70Δ* with either *tmn2Δ* or *tmn2Δ tmn3Δ* resulted in CPY secretion, showing that Emp70 is functionally redundant with Tmn2 in vacuolar protein sorting and that the Emp70 protein family is required for normal endosomal function.

Figure 7 Genetic interactions of sphingolipid metabolism. (a) Graphic representation of the sphingolipid synthesis pathway. Blue, negative genetic interactions; yellow, positive interactions. (b) Genes encoding enzymes acting in succession in sphingolipid synthesis show higher correlation than genes further apart in the metabolic network. For each gene pair in sphingolipid synthesis, the pathway distance of genes (that is, the number of metabolic intermediates between the catalyzed reactions) is plotted against the correlation coefficient of the gene pairs. The red line is a best-fit linear regression line fitted for all the data points on the graph.

Sphingolipid metabolism and its regulation

The plasma-membrane E-MAP interrogates relationships within metabolic networks that are important for plasma-membrane function, including sphingolipid metabolism (Fig. 2, inserts 3a and 3b, and Fig. 7a). Consistent with their common function, many of the sphingolipid pathway genes showed high correlation (>0.2). Figure 7b shows the distance of the action of enzymes in the pathway plotted against the correlation coefficient of the corresponding genes. The linear best fit on all data points revealed that genes encoding enzymes catalyzing subsequent steps are more highly correlated than genes further away in the metabolic network. Moreover, whereas most mutations in genes encoding enzymes catalyzing early steps of sphingolipid synthesis have negative genetic interactions with each other (Fig. 2, insert 3b, and Fig. 7a), they show positive genetic interactions when combined with mutations in genes acting late in complex sphingolipid formation (Fig. 2, insert 3a, and Fig. 7a). This might indicate that deficiency in late-acting enzymes leads to a buildup of toxic intermediates, which can be suppressed by deleting genes encoding upstream-acting enzymes. Precedence for this includes inhibition of Aur1, which converts ceramide to inositolphosphoceramide by aureobasidin A, leading to complex sphingolipids depletion and a concomitant accumulation of ceramide, which both contribute to toxicity⁴⁴.

The plasma-membrane E-MAP also revealed that *ROM2*, encoding a Rho1 GTPase exchange factor, has strong genetic connections to sphingolipid synthesis genes. For example, *ROM2* has correlated genetic profiles with *FEN1*, *SUR2*, *LCB3* and *SUR4*, all acting early,



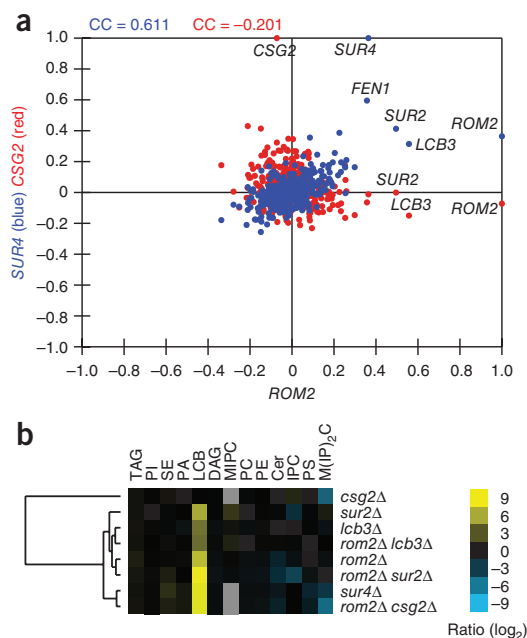


Figure 8 Rom2 interacts with sphingolipid metabolism. **(a)** Genes with correlating genetic profiles are shared between *SUR4* and *ROM2* but not between *CSG2* and *ROM2*. Correlation coefficients between the genetic profile of *ROM2* and each of the other 373 profiles in the E-MAP are plotted on the x axis against, on the y axis, either the similar set of values for the *SUR4* profile with all other profiles (blue) or those for *CSG2* with all other profiles (red). Labeled points indicate genes with profiles that are positively correlated with the profile of *ROM2* in blue and red indicate the correlation coefficients for the full set of blue or red points plotted. **(b)** Lipidome profiling of *rom2Δ* and selected sphingolipid metabolism mutants. Lipid class abundances were normalized to WT levels. Sterol esters (SE), phosphatidic acid (PA), triacylglycerol (TAG), long chain base (LCB) mannosylinositol phosphoceramide (MIPC), phosphatidylethanolamine (PE), diacylglycerol (DAG), phosphatidylcholine (PC), phosphatidylinositol (PI), ceramide (Cer), phosphatidylserine (PS) mannosylinositol-2-phosphoceramide (M(IP)₂C) and inositol phosphoceramide (IPC) levels are shown.

but shows negative correlation with *CSG2* acting late in sphingolipid synthesis (Fig. 8a). In addition, a *ROM2* deletion mutation results in a strong synthetic sick phenotype with *lcb3Δ*, *sur2Δ* *dpl1Δ* and *ysr3Δ*, all genes encoding enzymes catalyzing different steps of sphingolipid metabolism (interaction score < -2; see Fig. 2, insert 3b, and data not shown). Together, this suggests that Rom2 is an activator of sphingolipid metabolism. To test this model, we profiled the lipidome of *rom2Δ* and several other mutants in the sphingolipid pathway by ‘shotgun’ lipidomics⁴⁵. *ROM2* deletion resulted in a lipid phenotype similar to that of *sur2Δ* or *sur4Δ* cells (Fig. 8b and Supplementary Table 6). Particularly, *ROM2* deletion led primarily to accumulation of long chain bases and a small decrease of ceramides. This argues that Rom2 activates sphingolipid synthesis by regulating the conversion of long chain bases to ceramides.

DISCUSSION

The plasma-membrane E-MAP quantitatively describes interactions between genes involved in plasma-membrane processes. Together with previous studies, it shows that the E-MAP technology can be used to detect protein interactions and signaling pathways as well as to uncover complex biological connections. Here, we highlighted several examples of novel insights into plasma-membrane function derived from the E-MAP, focusing on its spatial organization and

homeostasis. As an example of a physical interaction revealed from the E-MAP data, we investigated *Eis1/Ymr031c* and defined it as an eisosome component. Based on its much lower abundance compared to the eisosome core components, it might have a special architectural or regulatory role there. This is also a case where we combined data from the plasma-membrane E-MAP with our visual screen for genes affecting *Pil1-GFP* localization³¹, which provides an example how the combination of different high-throughput datasets helps to uncover previously unrecognized relationships.

Mining of the plasma-membrane E-MAP also yielded information on more functional interactions not reflected in physical associations. The transmembrane protein *Emp70* has a fascinatingly complex localization and genetically interacts with eisosome components. Particularly intriguing is the *Emp70* pool localized in endosomal structures that often appear connected with the vacuolar membrane. This observation raises the possibility that endosomes reach out to the plasma membrane and pick up their cargo. It also suggests that at least parts of the endosomal membrane system might be a tubular network connected to the vacuole, but further detailed cell-biological studies will have to clarify this point.

We also used the plasma-membrane E-MAP to interrogate metabolic networks and their regulation. The strong correlation profiles of sphingolipid synthesis genes argues that novel functionally related genes could be found by using the genetic profiles from the plasma-membrane E-MAP. For example, genes that function in sphingolipid metabolism or are involved in its regulation would be expected to cluster with known sphingolipid synthesis genes. Using this logic, we identified *Rom2* as a regulator of sphingolipid metabolism. Mechanistically, its activator function could occur either through ceramide synthesis activation by *Rom2* or through negative regulation of ceramidase. Between these two hypotheses, we consider the first one more likely, as *rom2Δ* clusters with genes encoding ceramide synthase (*lag1Δ lac1Δ*) but not *ycd1Δ*, which encodes ceramidase (Fig. 2, insert 3b). This is consistent with previous findings that connect the *Tor2* kinase pathway with *Rho1*-signaling via *Rom2* as well as recent findings that *TORC2* is required for ceramide biosynthesis^{7,46}. This previous study⁷ implicated an alternative branch of *TORC2* signaling through the *Ypk2* kinase in regulation of ceramide biosynthesis but did not rule out involvement of *Rom2*. The effect of *ROM2* deletion could either be directly on ceramide synthase or, alternatively, could block the synthesis of its substrate, long chain fatty acid-CoA. In the latter model, the depletion of long chain fatty acids would slow ceramide synthesis and would therefore lead to the accumulation of long chain bases, the second substrate of ceramide synthase. In either scenario, *Rom2* has a stimulatory function in sphingolipid synthesis at the step converting long chain bases to ceramides. Consistent with this notion, the inhibition of sphingolipid synthesis by the antifungal drug *myriocin* leads to a relocalization of *Rom2* from the plasma membrane⁴⁷. *Rom2* is recruited to the plasma membrane through the binding of phosphoinositol-(4,5)-bisphosphate (PI(4,5)P₂) by its pleckstrin homology domain, and reduction of PI(4,5)P₂ also relocalizes *Rom2* (ref. 48). This raises the possibility that *Rom2* serves to connect phosphoinositide and sphingolipid signaling pathways. The details of this regulation of sphingolipid metabolism remain to be worked out, but it shows how genetic interactions in the plasma-membrane E-MAP yield novel insights into metabolic networks and their regulation.

We anticipate that this dataset will fuel many more mechanistic studies. In particular, integration with other data from lipidomics, interaction proteomics or systematic visual screens are likely to reveal novel insights into the regulation of plasma-membrane processes. In addition, many antifungal drugs target functions connected to the

plasma membrane, such as cell-wall and ergosterol synthesis. Probing the set of genes on the E-MAP presented here with a battery of drugs and comparing of the resulting drug profiles to the mutant profiles is an effective way to identify putative drug targets. This would facilitate the identification of compounds impinging on these various processes and could potentially have therapeutic value.

METHODS

Methods and any associated references are available in the online version of the paper at <http://www.nature.com/nsmb/>.

Note: Supplementary information is available on the Nature Structural & Molecular Biology website.

ACKNOWLEDGMENTS

We thank members of the Walther and Krogan laboratory for critical reading and comments, J. Brickner for suggestions, Ulrike Laabs for excellent technical assistance, O. Nørregaard Jensen (University of Southern Denmark) for providing access to the Nanomate Triversa used for the lipidomic experiments and P. Kemmeren for establishing the database. This work was supported by the Max Planck Society (T.C.W.), the German Research Foundation (DFG; T.C.W.), the German-Israeli Foundation (T.C.W.), the US National Institutes of Health, the Searle, Sandler and Keck Foundations (N.J.K.), the International Human Frontier Science Program (HFSP; T.C.W.), the Israel Science Foundation (grant no. 802/08; R.S.), the Edmond J. Safra Bioinformatics program at Tel Aviv University (I.U.), the Programa de Apoyo Sectorial a la Estrategia Nacional de Innovación (INNOVA URUGUAY, DCI-ALA/2007/19.040, P.S.A.), the Agencia Nacional de Investigación e Innovación (ANII, A.O.-C.), the Danish Council for Independent Research (DOK1155860, C.S.E.) and Lundbeckfonden (R45-A4342, C.S.E.).

AUTHOR CONTRIBUTIONS

All authors contributed to every aspect of this work.

COMPETING FINANCIAL INTERESTS

The authors declare no competing financial interests.

Published online at <http://www.nature.com/nsmb/>.

Reprints and permissions information is available online at <http://npg.nature.com/reprintsandpermissions/>.

1. Grossmann, G., Opekarova, M., Malinsky, J., Weig-Meckl, I. & Tanner, W. Membrane potential governs lateral segregation of plasma membrane proteins and lipids in yeast. *EMBO J.* **26**, 1–8 (2007).
2. Walther, T.C. *et al.* Eisosomes mark static sites of endocytosis. *Nature* **439**, 998–1003 (2006).
3. Grossmann, G. *et al.* Plasma membrane microdomains regulate turnover of transport proteins in yeast. *J. Cell Biol.* **183**, 1075–1088 (2008).
4. deHart, A.K., Schnell, J.D., Allen, D.A. & Hicke, L. The conserved Pkh-Ypk kinase cascade is required for endocytosis in yeast. *J. Cell Biol.* **156**, 241–248 (2002).
5. Friant, S., Lombardi, R., Schmelzle, T., Hall, M.N. & Riezman, H. Sphingoid base signaling via Pkh kinases is required for endocytosis in yeast. *EMBO J.* **20**, 6783–6792 (2001).
6. Walther, T.C. *et al.* Pkh-kinases control eisosome assembly and organization. *EMBO J.* **26**, 4946–4955 (2007).
7. Aronova, S. *et al.* Regulation of ceramide biosynthesis by TOR complex 2. *Cell Metab.* **7**, 148–158 (2008).
8. Guan, X.L. *et al.* Functional interactions between sphingolipids and sterols in biological membranes regulating cell physiology. *Mol. Biol. Cell* **20**, 2083–2095 (2009).
9. Tabuchi, M., Audhya, A., Parsons, A.B., Boone, C. & Emr, S.D. The phosphatidylinositol 4,5-bisphosphate and TORC2 binding proteins Slm1 and Slm2 function in sphingolipid regulation. *Mol. Cell Biol.* **26**, 5861–5875 (2006).
10. Tong, A.H. *et al.* Global mapping of the yeast genetic interaction network. *Science* **303**, 808–813 (2004).
11. Schuldiner, M. *et al.* Exploration of the miniarray and organization of the yeast early secretory pathway through an epistatic miniarray profile. *Cell* **123**, 507–519 (2005).
12. Collins, S.R., Schuldiner, M., Krogan, N.J. & Weissman, J.S. A strategy for extracting and analyzing large-scale quantitative epistatic interaction data. *Genome Biol.* **7**, R63 (2006).
13. Schuldiner, M., Collins, S.R., Weissman, J.S. & Krogan, N.J. Quantitative genetic analysis in *Saccharomyces cerevisiae* using epistatic miniarray profiles (E-MAPs) and its application to chromatin functions. *Methods* **40**, 344–352 (2006).
14. Ulitsky, I., Shlomi, T., Kupiec, M. & Shamir, R. From E-MAPs to module maps: dissecting quantitative genetic interactions using physical interactions. *Mol. Syst. Biol.* **4**, 209 (2008).
15. Bandyopadhyay, S., Kelley, R., Krogan, N.J. & Ideker, T. Functional maps of protein complexes from quantitative genetic interaction data. *PLoS Comput. Biol.* **4**, e1000065 (2008).
16. Collins, S.R. *et al.* Functional dissection of protein complexes involved in yeast chromosome biology using a genetic interaction map. *Nature* **446**, 806–810 (2007).
17. Fiedler, D. *et al.* Functional organization of the *S. cerevisiae* phosphorylation network. *Cell* **136**, 952–963 (2009).
18. Wilmes, G.M. *et al.* A genetic interaction map of RNA-processing factors reveals links between Sem1/Dss1-containing complexes and mRNA export and splicing. *Mol. Cell* **32**, 735–746 (2008).
19. Collins, S.R. *et al.* Toward a comprehensive atlas of the physical interactome of *Saccharomyces cerevisiae*. *Mol. Cell Proteomics* **6**, 439–450 (2007).
20. Gavin, A.C. *et al.* Proteome survey reveals modularity of the yeast cell machinery. *Nature* **440**, 631–636 (2006).
21. Krogan, N.J. *et al.* Global landscape of protein complexes in the yeast *Saccharomyces cerevisiae*. *Nature* **440**, 637–643 (2006).
22. Ren, G., Vajihala, P., Lee, J.S., Winsor, B. & Munn, A.L. The BAR domain proteins: molding membranes in fission, fusion, and phagy. *Microbiol. Mol. Biol. Rev.* **70**, 37–120 (2006).
23. Revardel, E., Bonneau, M., Durrens, P. & Aigle, M. Characterization of a new gene family developing pleiotropic phenotypes upon mutation in *Saccharomyces cerevisiae*. *Biochim. Biophys. Acta* **1263**, 261–265 (1995).
24. Breton, A.M. & Aigle, M. Genetic and functional relationship between Rvsp, myosin and actin in *Saccharomyces cerevisiae*. *Curr. Genet.* **34**, 280–286 (1998).
25. Brizzio, V., Gammie, A.E. & Rose, M.D. Rvs161p interacts with Fus2p to promote cell fusion in *Saccharomyces cerevisiae*. *J. Cell Biol.* **141**, 567–584 (1998).
26. Friesen, H. *et al.* Characterization of the yeast amphiphysins Rvs161p and Rvs167p reveals roles for the Rvs heterodimer *in vivo*. *Mol. Biol. Cell* **17**, 1306–1321 (2006).
27. Jonikas, M.C. *et al.* Comprehensive characterization of genes required for protein folding in the endoplasmic reticulum. *Science* **323**, 1693–1697 (2009).
28. Valdivia, R.H., Baggott, D., Chuang, J.S. & Schekman, R.W. The yeast clathrin adaptor protein complex 1 is required for the efficient retention of a subset of late Golgi membrane proteins. *Dev. Cell* **2**, 283–294 (2002).
29. Efe, J.A. *et al.* Yeast Mon2p is a highly conserved protein that functions in the cytoplasm-to-vacuole transport pathway and is required for Golgi homeostasis. *J. Cell Sci.* **118**, 4751–4764 (2005).
30. Levin, D.E. Cell wall integrity signaling in *Saccharomyces cerevisiae*. *Microbiol. Mol. Biol. Rev.* **69**, 262–291 (2005).
31. Frohlich, F. *et al.* A genome-wide screen for genes affecting eisosomes reveals Nce102 function in sphingolipid signaling. *J. Cell Biol.* **185**, 1227–1242 (2009).
32. Ong, S.E. *et al.* Stable isotope labeling by amino acids in cell culture, SILAC, as a simple and accurate approach to expression proteomics. *Mol. Cell Proteomics* **1**, 376–386 (2002).
33. Wang, H. *et al.* A complex-based reconstruction of the *Saccharomyces cerevisiae* interactome. *Mol. Cell Proteomics* **8**, 1361–1381 (2009).
34. Deng, C., Xiong, X. & Krutchinsky, A.N. Unifying fluorescence microscopy and mass spectrometry for studying protein complexes in cells. *Mol. Cell Proteomics* **8**, 1413–1423 (2009).
35. Schimmoller, F., Diaz, E., Muhlbauer, B. & Pfeffer, S.R. Characterization of a 76 kDa endosomal, multispansing membrane protein that is highly conserved throughout evolution. *Gene* **216**, 311–318 (1998).
36. Vida, T.A. & Emr, S.D. A new vital stain for visualizing vacuolar membrane dynamics and endocytosis in yeast. *J. Cell Biol.* **128**, 779–792 (1995).
37. Zheng, B., Wu, J.N., Schober, W., Lewis, D.E. & Vida, T. Isolation of yeast mutants defective for localization of vacuolar vital dyes. *Proc. Natl. Acad. Sci. USA* **95**, 11721–11726 (1998).
38. Babst, M., Wendland, B., Estepa, E.J. & Emr, S.D. The Vps4p AAA ATPase regulates membrane association of a Vps protein complex required for normal endosome function. *EMBO J.* **17**, 2982–2993 (1998).
39. Teis, D., Saksena, S. & Emr, S.D. Ordered assembly of the ESCRT-III complex on endosomes is required to sequester cargo during MVB formation. *Dev. Cell* **15**, 578–589 (2008).
40. Brickner, J.H. & Fuller, R.S. S011 encodes a novel, conserved protein that promotes TGN-endosomal cycling of Kex2p and other membrane proteins by modulating the function of two TGN localization signals. *J. Cell Biol.* **139**, 23–36 (1997).
41. Sipos, G. *et al.* Soi3p/Rav1p functions at the early endosome to regulate endocytic trafficking to the vacuole and localization of trans-Golgi network transmembrane proteins. *Mol. Biol. Cell* **15**, 3196–3209 (2004).
42. Robinson, J.S., Klionsky, D.J., Banta, L.M. & Emr, S.D. Protein sorting in *Saccharomyces cerevisiae*: isolation of mutants defective in the delivery and processing of multiple vacuolar hydrolases. *Mol. Cell Biol.* **8**, 4936–4948 (1988).
43. Rothman, J.H., Howald, I. & Stevens, T.H. Characterization of genes required for protein sorting and vacuolar function in the yeast *Saccharomyces cerevisiae*. *EMBO J.* **8**, 2057–2065 (1989).
44. Cerantola, V. *et al.* Aureobasidin A arrests growth of yeast cells through both ceramide intoxication and deprivation of essential inositolphosphorylceramides. *Mol. Microbiol.* **71**, 1523–1537 (2009).
45. Ejsing, C.S. *et al.* Global analysis of the yeast lipidome by quantitative shotgun mass spectrometry. *Proc. Natl. Acad. Sci. USA* **106**, 2136–2141 (2009).
46. Schmidt, A., Bickle, M., Beck, T. & Hall, M.N. The yeast phosphatidylinositol kinase homolog TOR2 activates RHO1 and RHO2 via the exchange factor ROM2. *Cell* **88**, 531–542 (1997).
47. Kobayashi, T., Takematsu, H., Yamaji, T., Hiramoto, S. & Kozutsumi, Y. Disturbance of sphingolipid biosynthesis abrogates the signaling of Mss4, phosphatidylinositol-4-phosphate 5-kinase, in yeast. *J. Biol. Chem.* **280**, 18087–18094 (2005).
48. Audhya, A. & Emr, S.D. Stt4 PI 4-kinase localizes to the plasma membrane and functions in the Pkc1-mediated MAP kinase cascade. *Dev. Cell* **2**, 593–605 (2002).



ONLINE METHODS

E-MAP analysis. Generation and analysis of the quantitative genetic interaction data was carried out as previously described^{11–13}.

Detection of functional modules. Modules were identified using an algorithm described previously¹⁴, which was applied to the S-scores in the plasma membrane E-MAP and a PPI network containing 49,010 interactions between 5,815 yeast genes, compiled from several databases^{49–51}. The algorithm identifies a collection of modules and a set of module pairs by optimizing a probabilistic scoring function. This function takes into account both similarities of the S-score profiles and the raw S-scores by preferring modules of genes having high correlation coefficients (CC-scores) between members of the same complex and negative S-scores among members of a module pair. The significance of the CC-scores and S-scores was assessed by fitting Gaussian distributions using an expectation-maximization algorithm.

Yeast strains and culture. All yeast strains used are listed in **Supplementary Table 7**. C-terminal fusions and gene deletions were generated by homologous recombination of PCR-generated DNA fragments⁵². All single-, double- or triple-deletion strains were confirmed by PCR. Strains expressing tagged proteins were confirmed by PCR and fluorescence microscopy or western blot. Yeast cells were grown according to standard procedure. For SILAC labeling, Pil1-TEV-GFP-expressing and WT yeast cells were grown in the presence of 20 mg l⁻¹ L-lysine-U-¹³C₆, ¹⁵N₂ and normal L-Lysine, respectively, with at least ten doublings to an OD₆₀₀ = 0.7.

Microscopy. Cells were grown to an OD₆₀₀ = 0.6 in synthetic medium at 30 °C unless indicated. Cells were mounted in synthetic media onto concanavalin A coated cover slips and imaged with an ANDOR/iXonEM 897 EM CCD camera and an Olympus 100× 1.4 NA oil immersion objective. We collected 16-bit images using Andor Image iQ 1.9 in the linear range of the camera. For presentation, images were filtered with a smoothing filter averaging 2 pixels, converted to 8-bit images and cropped using ImageJ (<http://rsb.info.nih.gov/ij/>). For quantitation of colocalization, we collected stacks and extracted four-dimensional images for individual cells. The area of overlap was quantified dividing the total area of the Emp70 signal by the area of overlap determined using the RG2B colocalization ImageJ plugin.

FM4-64 uptake assay. Cells exponentially growing at an OD₆₀₀ = 0.7 (1 ml) were harvested, resuspended in 50 µl of medium and chilled on ice for 5 min. FM4-64 was added to a final concentration of 10 µM and incubated for another 10 min. Cells were washed with ice-cold medium, resuspended and incubated for different time points, after which cells were killed by 10 mM NaN₃ and 10 mM NaF and immediately analyzed by microscopy.

CPY secretion assay. The CPY secretion colony blot assay was performed as described using anti-CPY antibodies (Invitrogen-A6428)⁵³.

Proteomics. Protein extracts from 70 ODs of 'light' and 'heavy' labeled cells were obtained as described³¹. For immunopurification, equivalent amounts of proteins were incubated with anti-GFP AB-conjugated magnetic nanobeads (Miltenyi Biotec) for 5 min at 4 °C and loaded on µMacs columns (Miltenyi Biotec) in a magnetic µMacs Separator (Miltenyi Biotec), washed three times with 1 ml of lysis buffer with 1% (v/v) Triton-X100, three times with 1 ml of lysis buffer without Triton-X100 and eluted by TEV cleavage. Eluates were mixed, diluted 5× in 8 M urea, reduced for 20 min at room temperature (22 °C) in 1 mM DTT and then alkylated for 30 min by 5.5 mM iodoacetamide in the dark. Then, the eluates were

digested, desalted and concentrated as described³¹. Peptides were separated online using an Easy nLC system (Proxeon Biosystems, Odense, Denmark). Samples (5 µl) were loaded as described³¹. Peptides were eluted with a segmented gradient of 2–60% solvent B over 102 min with a constant flow of 250 nl min⁻¹. The HPLC system was coupled to an LTQ-Orbitrap Velos mass spectrometer (Thermo Fisher Scientific) via a nanoscale LC interface (Proxeon Biosystems). The spray voltage was 2.2 kV, and the temperature of the heated capillary was 180 °C. Survey full scan spectra (*m/z* = 300–1600) were acquired in positive ion mode with a resolution of 60,000 at *m/z* = 400 after accumulation of 1,000,000 ions. Up to ten most-intense ions were sequenced by collision-induced dissociation in the LTQ. Precursor ion charge-state screening was enabled, and all unassigned charge states as well as singly charged peptides were rejected. The dynamic exclusion list was restricted to a maximum of 500 entries with a maximum retention period of 90 s and a relative mass window of 10 p.p.m. Orbitrap measurements were performed enabling the lock mass option for survey scans to improve mass accuracy⁵⁴. Data were acquired using the Xcalibur software (version 2.1.0, Thermo Fisher Scientific) and MaxQuant, version 1.0.1 (ref. 55). The data was searched against the yeast database concatenated with reversed copies of all sequences^{56,57} and supplemented with frequent contaminants using Mascot (version 2.2.0, Matrix Science⁵⁸). Carbamidomethylated cysteines were set as fixed, whereas oxidation of methionine and N-terminal acetylation were set as variable modifications. Maximum allowed mass deviation for MS/MS peaks and missed cleavages were 0.5 and 3 Da, respectively. Maximum false-discovery rates (FDR) were 0.01 both on peptide and protein levels. Minimum required peptide length was 6 residues. Proteins with at least two peptides were considered identified.

Lipidomics. Cell were harvested from 20 ml logarithmically growing cultures in synthetic medium at 30 °C and washed in water at 4 °C. Cell pellets were frozen immediately in liquid nitrogen and were thawed later by adding 155 mM NH₄HCO₃ (pH 8), followed by cell disruption using zirconia beads (0.5 mm; BioSpec Products). Lipids were extracted from lysates as previously described⁴⁵ and analyzed using a LTQ Orbitrap XL mass spectrometer (Thermo Fisher Scientific) equipped with a robotic nanoflow ion source TriVersa NanoMate (Advion BioSciences Ltd.). MS survey scans were acquired in positive and negative ion mode using the Orbitrap analyzer with target mass resolution of 100,000 and automatic gain control set at 1e⁵ as the target value⁴⁵.

49. Cherry, J.M. *et al.* SGD: *Saccharomyces* Genome Database. *Nucleic Acids Res.* **26**, 73–79 (1998).
50. Kanehisa, M. & Goto, S. KEGG: Kyoto encyclopedia of genes and genomes. *Nucleic Acids Res.* **28**, 27–30 (2000).
51. Reguly, T. *et al.* Comprehensive curation and analysis of global interaction networks in *Saccharomyces cerevisiae*. *J. Biol.* **5**, 11 (2006).
52. Janke, C. *et al.* A versatile toolbox for PCR-based tagging of yeast genes: new fluorescent proteins, more markers and promoter substitution cassettes. *Yeast* **21**, 947–962 (2004).
53. Mullins, C. & Bonifacino, J.S. Structural requirements for function of yeast GGAs in vacuolar protein sorting, α -factor maturation, and interactions with clathrin. *Mol. Cell. Biol.* **21**, 7981–7994 (2001).
54. Olsen, J.V. *et al.* Parts per million mass accuracy on an Orbitrap mass spectrometer via lock mass injection into a C-trap. *Mol. Cell. Proteomics* **4**, 2010–2021 (2005).
55. Cox, J. & Mann, M. MaxQuant enables high peptide identification rates, individualized p.p.b.-range mass accuracies and proteome-wide protein quantification. *Nat. Biotechnol.* **26**, 1367–1372 (2008).
56. Moore, R.E., Young, M.K. & Lee, T.D. Qscore: an algorithm for evaluating SEQUEST database search results. *J. Am. Soc. Mass Spectrom.* **13**, 378–386 (2002).
57. Peng, J., Elias, J.E., Thoreen, C.C., Licklider, L.J. & Gygi, S.P. Evaluation of multidimensional chromatography coupled with tandem mass spectrometry (LC/LC-MS/MS) for large-scale protein analysis: the yeast proteome. *J. Proteome Res.* **2**, 43–50 (2003).
58. Perkins, D.N., Pappin, D.J., Creasy, D.M. & Cottrell, J.S. Probability-based protein identification by searching sequence databases using mass spectrometry data. *Electrophoresis* **20**, 3551–3567 (1999).